Philosophical Transactions of the Royal Society A-Mathematical Physical and Engineering Sciences, 2009, Vol. 367, Issue 1899, pp2985-2997.

Large Eddy Simulation Using High Resolution and High Order Methods

By D.Drikakis, M.Hahn, A. Mosedale & B.Thornber †

Fluid Mechanics & Computational Science Group
Department of Aerospace Sciences
Cranfield University, UK

Restrictions on computing power make Direct Numerical Simulation too expensive for complex flows, and Reynolds Averaged Navier Stokes simulations are easily computed but inaccurate for large classes of flows. Due to these driving forces there is a need for accurate Large Eddy Simulation (LES) methods which are industrially applicable and efficient. This paper reviews recent findings about the leading order dissipation rate associated with high-resolution methods, and improvements to the standard schemes for use in highly turbulent flows. Results from Implicit LES are presented for a broad range of flows and numerical schemes ranging from the second-order MUSCL to very high-order (up to 9th order) WENO schemes.

Keywords: Place keywords here

1. Introduction

As current computational power does not allow Direct Numerical Simulation (DNS) of complex flows, LES has emerged as a viable alternative where the time dependent behaviour of the flow must be resolved. Conventional LES, where an explicit subgrid model is added to the averaged Navier-Stokes equations, has been employed successfully in many prototype flows, however it is known to provide excessive dissipation in flows where the growth of an initially small perturbation to fully turbulent flow must be resolved (Lesieur & Metais (1996); Pope (2000)). It has been recognised that some numerical schemes gain good results in complex flows without the explicit addition of a subgrid model (Lesieur & Metais (1996)). This occurs when the subgrid model is implicitly designed into the limiting method of the numerical scheme, based on the observation that an upwind numerical scheme can be rewritten as a central scheme plus a dissipative term (see Drikakis (2003); Drikakis & Rider (2004); Grinstein *et al.* (2007) and references therein). Such implicit subgrid models fall into the class of structural models, as there is no assumed form of the nature of the subgrid flow thus the subgrid model is entirely determined by the structure of the resolved flow (Sagaut (2001)).

A major challenge facing Implicit LES is the development of a theoretical framework which justifies of the use of the truncation error of the numerical scheme as a sub-grid model, and guides structured development of numerical methods. The first important element of such a theoretical justification is to consider the requirements on the numerical scheme dependent on how well resolved the physical problem is. By considering numerical resolution there are two clear categories of Implicit LES.

† Authors' names appear in alphabetical order

The first category relates to the behaviour of the numerical solution when the simulation is well resolved. In this case the grid resolution and numerical methods are combined in such a way that the large scales present in the problem are fully resolved by the numerical method with negligible influence of numerical viscosity. To ensure a reasonable result, the numerical scheme must also resolve accurately the vortices which interact the strongest with the large scales, i.e. the neighbouring modes. A final requirement exists in the case of transitional flows, where the numerical method must have adequate resolution to capture the initial perturbations which become unstable and trigger turbulence in the problem (a requirement for all LES). An excellent example of an ILES which falls in the category is that of Cohen *et al.* (2002), where a fundamental flow instability is simulated using very high grid resolutions - thus isolating the scales of interest from the dissipative scales.

If these three criteria are satisfied then the level and form of the numerical dissipation should not significantly influence the problem. The basis of this assumption is an application of Kolmogorov's hypothesis - where it was shown that the appearance of a sub-inertial range relies only on adequate separation between the start of the inertial range and the dissipative scales - it does not rely on the form of the dissipation. In an analogous situation as long as there is such a separation between the scales which influence the energetic scales, and the scales dissipated by the numerical method then an Implicit Large Eddy Simulation should give a correct result. It should be stated that an initial assumption in the Large-Eddy approximation is that the flow quantities of interest are controlled by the large scales - this is not always the case (e.g. reactive flows).

This first category of ILES has a relatively simple framework, so long as the user is aware of the resolution requirements of their particular numerical scheme - e.g. how many computational cells are required to capture a single mode/vortex. This approach suggests the use of very high order schemes which focus the dissipation into a narrow band at high wavenumbers, thus allowing an independent regime to evolve. It would also be beneficial it that it would improve the scheme's ability to be able to resolve initial perturbations in the flow field which then either trigger or promote turbulent fluctuations.

The second category of ILES emerges when there is an insufficient separation of the large and dissipative scales. This occurs frequently in complex industrial flows where Very Large Eddy Simulation is commonplace. In this case it is desirable that the numerical method provide a dissipative influence on the large scales mimicking that produced by the scales which they would normally interact with if the full spectrum was present. This is the regime where both classical LES and Implicit LES encounter difficulties as the simulation is now sensitive to the form of the imposed subgrid model.

At this point there are a plethora of classical LES models which can be applied to the problem, and an equally large number of ILES numerical methods. The required form of the dissipation is usually derived using a closure assumption such as the eddy-viscosity hypothesis - and the coefficients calibrated to give the required results in classical test cases such as homogeneous decaying turbulence. Interestingly, studies by Meyers *et al.* (2007) have shown that the optimum coefficients for LES are often functions of the choice of grid resolution and numerical filter size. Improvements in specification of the coefficients by using dynamic procedures often

give improvements only in areas of the flow where the LES model is not strictly applicable (such as near walls, transitional regions, laminar flow) (Pope (2004)).

A clear uncertainty in this area is the universality of the approach when applied to many different flows. For example, it is not certain to what extent anisotropy persists into the beginnings of the inertial range, which is likely to have an influence on the form of the energy spectrum, the magnitude of second order statistics and hence the dissipation rate (Casciola *et al.* (2007)). In these situations a model which is based on the assumption of homogeneous turbulence at the high wavenumbers could not be expected to be accurate. This argument is equally applicable to ILES methods. Given the uncertainties involved, this second category of LES is certainly by far the most challenging. The vast majority of ILES simulations fall into this category, principally due to the massive computational requirement for highly resolved simulations. This includes open cavity flow (Thornber & Drikakis (2008); Hahn & Drikakis (2005); Drikakis (2003); Larcheveque *et al.* (2003)), geophysical flows (Margolin *et al.* (1999); Smolarkiewicz & Margolin (1998)), delta wings (Gordnier & Visbal (2005)) and low resolution (less than 128^3) decaying turbulence (Drikakis *et al.* (2006); Fureby *et al.* (1997); Porter *et al.* (1998); Fureby & Grinstein (2002); Margolin *et al.* (2002); Hickel *et al.* (2006); Thornber *et al.* (2007)).

The theoretical analysis of incompressible flow simulations using Modified Equation Analysis (MEA), particularly the influence of Finite Volume schemes has been investigated by (Drikakis & Rider (2004); Margolin *et al.* (2006); Margolin & Rider (2005); Grinstein *et al.* (2007)). These papers emphasised the importance of the finite volume approach in that it allows the natural evolution of volume averaged quantities - i.e. the filtered quantities necessary in LES. Numerical methods for incompressible flows can be fairly flexible in that they do not require strict monotonic behaviour to give numerical stability. Often favourable numerical methods for turbulence to do not conserve the positivity of passive scalars - something which requires additional monotonicity constraints. However, the flexibility allows for a greater scope of optimisation of the numerical stencil to provide favourable dissipative properties. An excellent example of this is the Approximate Deconvolution Methods proposed by (Hickel *et al.* (2006)), where the weightings for the variable reconstruction are chosen to give as close as possible behaviour to a spectral eddy viscosity.

In compressible methods there is significantly less room for manoeuvre. The numerical method must be monotonic in the thermodynamic quantities (density and pressure) in order to remain stable, i.e. so that the simulation doesn't crash. This stability is usually added as explicit diffusion terms such as in the Jameson scheme (Jameson *et al.* (1981)), or through upwinding of the fluxes, as employed in the Godunov method (Godunov (1959)). This is especially important in the simulation of multi-component flows where overshoots in the mass or volume fraction can lead to the prediction of negative densities or extremely unphysical equations of state (e.g. ratio's of specific heats less than one for a perfect gas equation of state).

It has been highlighted that upwind methods are typically overly-dissipative for simulations of homogeneous decaying turbulence when using second and third order methods (Garnier *et al.* (1999)). Resorting to very higher order methods improves the situation, however it does not cure the problem completely (Thornber *et al.* (2007)). Higher order methods will give reasonable results in terms of growth of the

length scales and kinetic energy dissipation rate, however the spectra are dissipative at the high wavenumbers (Thornber *et al.* (2007)).

Analysis of the source of the dissipation of turbulent kinetic energy in upwind schemes reveals a remarkably simple relationship. The absolute dissipation of fluctuating kinetic energy is proportional to the temperature multiplied by the change of entropy (assuming an approximately isothermal flow) (Thornber *et al.* (2008*a*)). This neglects the 'apparent' dissipation of kinetic energy caused by isentropic transformation of kinetic energy to internal energy in the form of local compressions and expansions. Using MEA, the evolution of entropy can be derived for a given compressible numerical scheme. This method has been developed in Thornber *et al.* (2008*a*) and demonstrates that the overly dissipative behaviour observed in simulations of homogeneous decaying turbulence can be ascribed to numerical dissipation which is proportional to the speed of sound. This excess dissipation delays the appearance of a sub-inertial range until much higher grid resolutions.

Taking this into account, the reconstruction method can be modified to ensure that the dissipation rate becomes constant at low Mach (Thornber *et al.* (2008*b*)). The key element to removing the adverse effects of low Mach number dissipation is to progressively central difference the velocity components as Mach number tends towards zero - which removes the speed of sound dependence of numerical dissipation as shown theoretically and numerically in (Thornber *et al.* (2008*b*)).

What remains is a dissipation rate proportional to the velocity increment cubed divided by the cell length in a similar functional form to the required dissipation rate for a turbulent subgrid model ($\propto u^3/l$) - which is constant in Mach. The modified numerical method is still monotone hence maintains the positivity of scalar quantities and has no noticeable difference in stability. The following sections will examine the influence of the order of accuracy and implementation of the improved version of the numerical method for three test cases ranging from the canonical case of homogeneous decaying turbulence, to applied Computational Aero-acoustics, flow over a swept wing, and shock induced turbulent mixing. It will also highlight the benefits from moving to higher order of accuracy numerical methods as compared to the classical second order upwind methods.

2. Homogeneous Decaying Turbulence

Turbulence remains the greatest challenge in fluid modelling. Most practical applications will involve low mach number turbulence and so it is important to test the ILES method in this respect. Much work has been done both experimentally and with Direct Numerical Simulation on simulating the decay of a homogeneous cube of turbulence Orzag & Patterson (1972), against the various theories that have been developed regarding turbulence - notably the well-established work of Kolmogorov Kolmogorov (1941, 1962). Results have been mixed, with no real consensus on many key parameters. It is instructive therefore to see where ILES falls within the range for a number of these measures of flow, and how the improved numerical method affects these results.

The problem has been simulated in line with previous work (Thornber *et al.* (2007)). In this section the turbulent kinetic energy spectra are presented as this is usually a weakness in ILES using shock capturing methods. It should be noted in addition to the results presented here that analysis of the growth of the integral

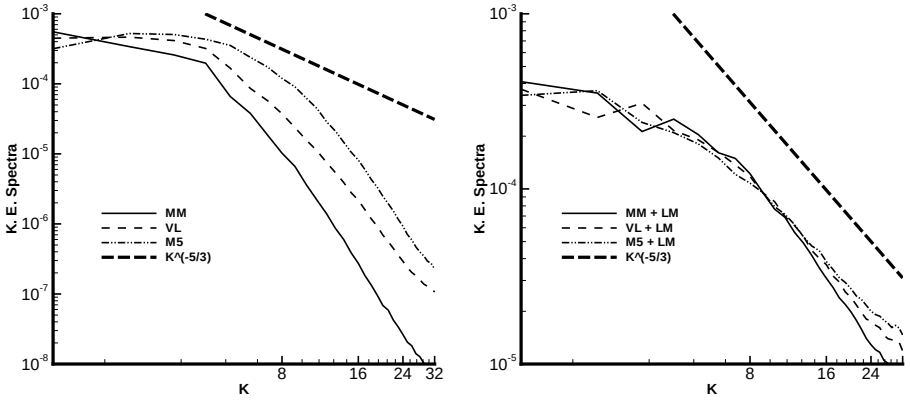

(a) No Low Mach Correction (b) With Low Mach Correction

Figure 1. Kinetic Energy spectra for different reconstruction methods at a given point in time with and without Low Mach (LM) correction

length scales, and dissipation of turbulent kinetic energy shows that they are within the bounds expected from experiment and theory.

Figure 1 shows the three-dimensional kinetic energy spectra for the different methods. Here we can now distinguish between the general dissipation related to the limiting method and the much more radical physical change in the structure of the flow gained by correcting for the low mach number dissipation. Kolmogorov's theory suggests the iniertial range of the cascade ought go with $k^{-\frac{5}{3}}$, as represented in the results by the heavy dashed line. On this relatively coarse grid the flow is conventionally under-resolved with the more dissipative methods however the improved method allows for small scales to be captured giving a much better correlation with theory over the entire flow.

3. Deep, Open Cavity Flow

Forestier *et al.* (2003) investigated the flow over an open cavity with a Length:Depth ratio of $1:2.4$ at a Reynolds number based on cavity length of $860,000$ and Mach 0.8. They measured mean and fluctuating velocity components, and in addition the sound pressure level spectrum at a single point located at $z/L = -0.7$. This case is ideal for the validation of compressible LES methods as it includes a strong shear layer, low Mach number perturbations within the cavity, and strong acoustic waves. In addition, the fundamental frequencies are not described well by Rossiter's theory without modifying the co-efficients away from the recommended values.

The results presented in this section were generated using a finite volume Godunov method employing the improved fifth-order in space reconstruction method (Thornber *et al.* (2008*b*)) with a HLLC approximate Riemann solver. Time stepping is achieved using a third order accurate Runge-Kutta method (Spiteri & Ruuth (2002)). Three grids were employed of 0.8, 1.4 and 3 million grid points respectively, as employed in Thornber & Drikakis (2008). An additional simulation was conducted at the coarse grid resolution using the standard fifth order MUSCL scheme. It should be stated that while the modified reconstruction method improves the

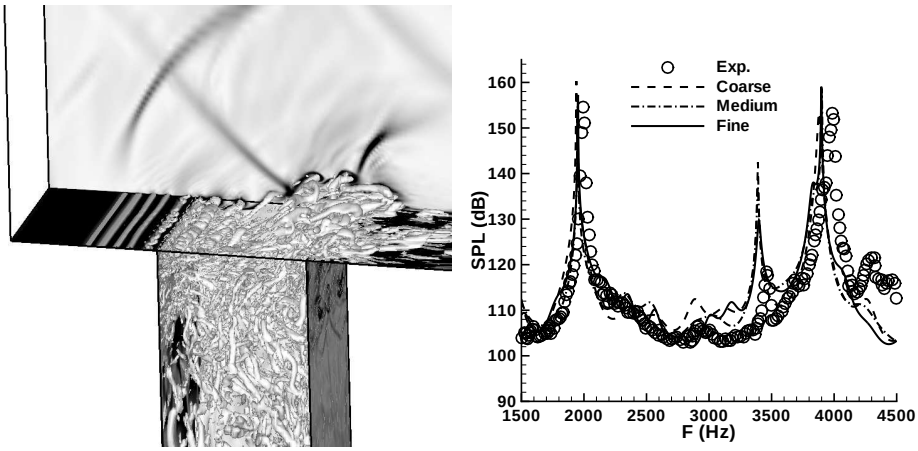

(a) (b)

Figure 2. (a) Close up of the cavity, showing visualisation of isosurfaces of $Q = 0.5 \times 10^6$. Contour flood shows pseudo-schlieren field ($|\nabla\rho|$). (b)Pressure power spectrum highlighting the dominant acoustic modes

resolution of fine scale features within the cavity and shear layer, the large coherent structures themselves are driven by a relatively high Mach number flow. Hence, the standard fifth order method also gains good results in terms of mean and fluctuating velocity components, as it still captures the large eddies with reasonable accuracy on these grids. Figure 2 shows flow visualisations consisting of isosurfaces of 'Q' criteria (Jeong & Hussain (1995)),

$$Q = -\frac{1}{2}\frac{\partial u_i}{\partial x_j}\frac{\partial u_j}{\partial x_i}, \tag{3.1}$$

where u_i are the Cartesian fluid velocities and x_i the Cartesian coordinates, which highlight the turbulent nature of the flow. Figure 2(b) shows the predicted and experimental sound pressure levels. Both sets of results demonstrate that the numerical approach employed here adequately represents the turbulent flow physics for both the mean flow velocities and Reynolds stresses.

Figure 3 shows typical results for the mean and fluctuating velocites over the shear layer for the three grid levels using the improved reconstruction method at $x/L = 0.6$ (where $x = 0$ is at the leading edge of the cavity). Comparisons with experiment at $x/L = 0.05$, 0.2, 0.4, 0.8 and 0.95 give a similar level of agreement.

Indeed, the discrepancies present are due to the initial specification of the boundary layer at the inlet, which is slightly too large. This leads to a thicker boundary layer at the leading edge of the cavity, thus increasing the height of the centre of the shear layer as can be seen from the points of maximum Reynolds stress in Figure 3. The sound pressure levels are predicted to within 6dB for all grid resolutions and within 2% of the experimentally measured frequency.

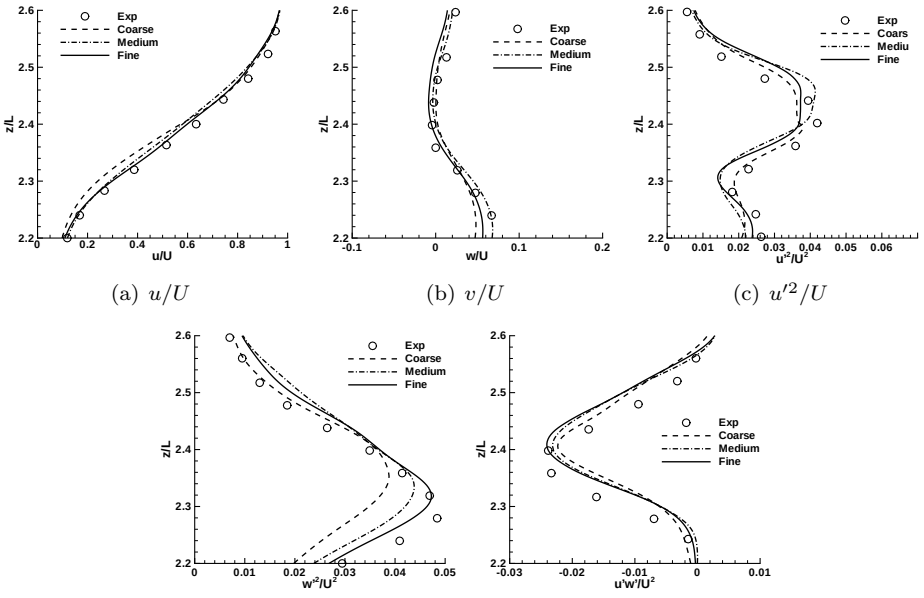

(a) u/U (b) v/U (c) u'^2/U

(d) w'^2/U (e) $u'w'/U$

Figure 3. Comparison of ILES results compared to experimental results of Forestier et al. Forestier *et al.* (2003) for $x/L = 0.6$

4. Swept Wing Flow

Swept and delta wings are of strong practical interest to aeronautical engineers as they can be found in all modern aircrafts travelling at transonic or supersonic speeds. At present, there are no theoretical models capable of predicting the characteristic leading edge separation with any degree of certainty, nor can the nature of the leading edge vortex breakdown observed in swept wing flow be convincingly explained. The complexity of the flow field makes it also extremely challenging to predict with any numerical method.

Within the framework of the MSTTAR Defence Aerospace Research Partnership (DARP) the flow around a swept wing at an angle of attack of 9° has been simulated with the present ILES approach using high-resolution methods for a Reynolds number of $210,000$ and a near incompressible Mach number of 0.3 (Hahn (2008)). The computational grid employed comprises 12.7M points, which is approximately half of what has been used in a conventional hybrid RANS/LES of the identical case (Li & Leschziner (2007)). Furthermore, third-order accuracy in space has been achieved by a MUSCL reconstruction method (Zoltak & Drikakis (1998)) and the integration in time has been realised by a third-order Runge-Kutta scheme with extended stability region (Drikakis & Rider (2004)).

The general physics of this problem has been captured in the ILES simulation as can be demonstrated by the instantaneous flow visualisation shown in Figure 4. The flow topology reveals separation along the leading edge of the swept wing, subsequent formation of the characteristic vortex roll-up and vortex breakdown near the wing tips. Moreover, the time-averaged velocity and turbulent kinetic energy profiles in the fully separated, turbulent region near the wing tip (90% half-span and

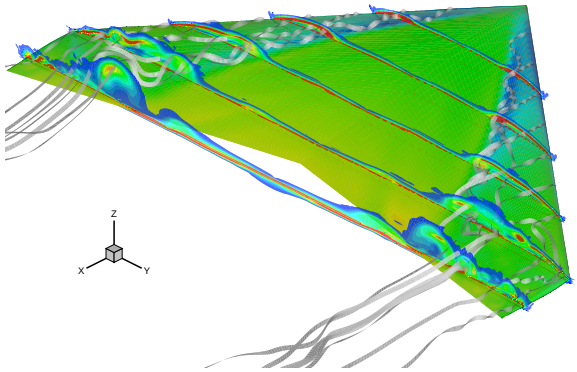

Figure 4. Instantaneous streamlines, slices of iso-vorticity contours and pressure coefficient distribution on the suction side of the wing

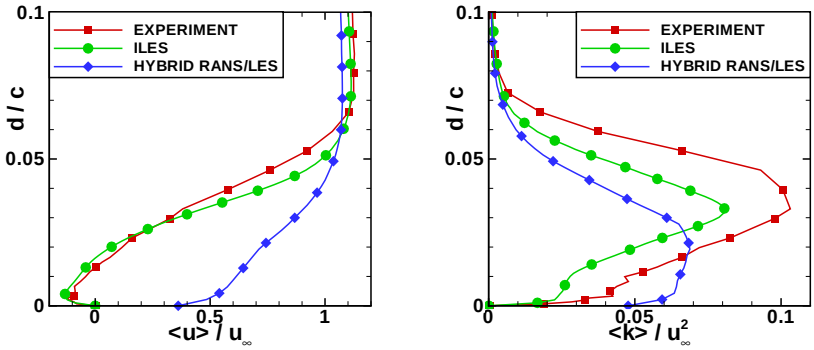

(a) Velocity profile (b) Turbulent energy profile

Figure 5. Comparison of averaged streamwise velocity and turbulent energy profiles at 90% half-span and 50% local chord

50% local chord), presented in Figure 5, provide insight into the quality of the ILES simulation. Here, data from the LES using the third-order high-resolution method (ILES) (Hahn (2008)) and from a hybrid RANS/LES simulation (Li & Leschziner (2007)) are compared against experiment (S. Zhang 2006, personal communication). Despite using more than 24M grid points, the hybrid RANS/LES fails to predict the flow separation. Consequently, the results for the turbulent kinetic energy disagree strongly with the experimental data. The velocity obtained by ILES, on the other hand, is nearly identical to the experiment. Although the magnitude of the turbulent kinetic energy is slightly lower, the high-resolution method is able to predict the correct shape of the profile.

5. Turbulent Mixing Experiment: Double Bump

The ILES approach has also been applied to complex multi-component turbulent mixing problems. The test case presented in this section corresponds to AWE's shock-tube experiment featuring a Richtmyer-Meshkov instability (RMI) arising

from an initial large-scale 2D double-bump perturbation at the interface between two gases (Holder *et al.* (2003)).

Various reconstruction methods ranging from second to ninth order have been investigated in conjunction with the HLLC approximate Riemann solver (Toro (1997)) and a third-order accurate TVD Runge-Kutta time-marching algorithm (Drikakis & Rider (2004)). Spatial high-resolution is achieved by using one of the following standard schemes: second order MUSCL van Albada (VA) (Toro (1997)), third order extended MUSCL van Albada (M3) (Zoltak & Drikakis (1998)), fifth order MUSCL (M5) (Kim & Kim (2005)), ninth order WENO (W9) (Balsara & Shu (2000)), or their improved counterparts VALM, M3LM, M5LM, W9LM incorporating the low Mach modification (Thornber *et al.* (2008*b*)). The linear shock-tube problem is discretised on a Cartesian grid comprising $160 \times 80 \times 40$ cells which corresponds to a uniform grid spacing of $\Delta = 1/4\,\mathrm{cm}$. A successive grid refinement study up to $\Delta = 1/16\,\mathrm{cm}$ has also been performed, but will not be discussed in detail.

The initial condition, shown as 2D slice in Figure 6, is given by a SF_6 region (dark) encased in air (light) with the large-scale perturbation on the right-hand interface. As the incident shock wave of Mach 1.26 passes from left to right, the membranes separating the two fluids rupture and the gases begin to mix. The shock wave reflected from the end wall decelerates the SF_6 layer and a high degree of turbulent mixing can be observed, see 3D structures in Figure 6 representing constant values of volume fraction.

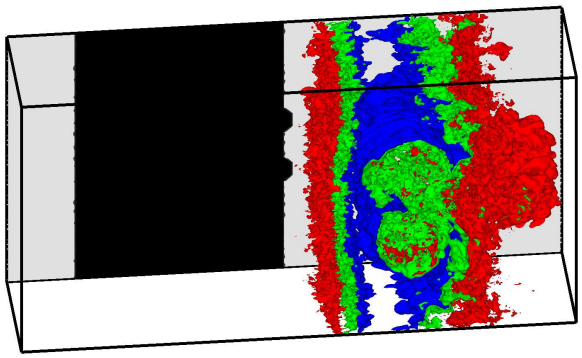

Figure 6. 3D contours of volume fraction and 2D slice of the initial condition

Results from the present simulations can be compared qualitatively with the experiment (Holder *et al.* (2003)), see Figure 7. Here, the experimental data is represented by the black lines overlaid on top of the 2D-averaged volume fraction and SF_6 density contours obtained with the improved fifth order method (M5LM) at identical times. As shown in Figure 7, the air/SF_6 interface and the shock position are in very good agreement with the experiment. Plots from other reconstruction methods have been omitted because they all yield similar results with minor differences regarding the location and the shape of the spike. However, the results obtained with different methods seem to converge as grid resolution improves.

The large-scale flow development in the simulations can also be validated quantitatively against experiment. For this purpose, the location of the bubble and the

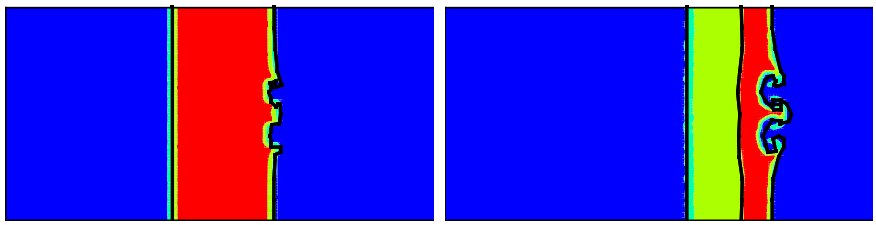

(a) Contours of volume fraction at T=1.26ms

(b) Contours of SF_6 density at T=1.90ms

Figure 7. Comparison of 2D-averaged contour levels as predicted by M5LM with the interface and shock position revealed by experiment (black lines)

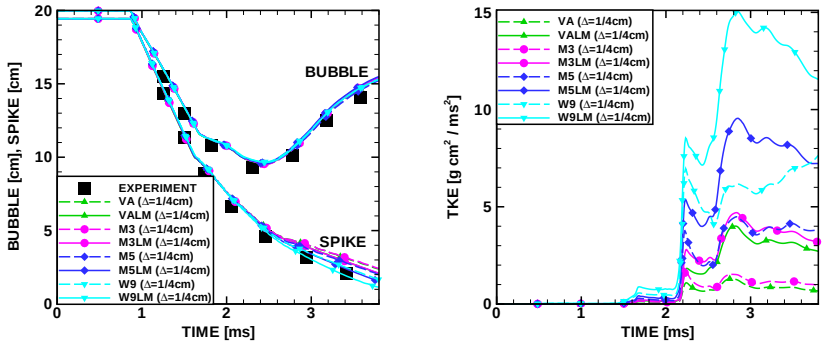

(a) Position of bubble/spike

(b) Turbulent kinetic energy

Figure 8. Development of bubble/spike position and turbulent kinetic energy

spike is presented in Figure 8(a) as the distance between the end plate of the shock-tube and the characteristic interface position. The interface position is given by the left edge and the right edge of the large bubbles and the tip of the spike, respectively. In accordance with the previous statement, all methods yield locations in good agreement with the large-scale features observed in experiment. Moreover, regardless of the reconstruction employed, the low Mach modification leads to improved results for the late-time spike position, i.e. T>2.5ms. The grid refinement study revealed that the locations predicted by all methods seem to converge to the experimental values.

The development of integral turbulent kinetic energy (TKE), provided in Figure 8(b), gives further evidence for the improvement at later times due to the low Mach modification. Its effect is reflected clearly by the increase in turbulent energy observed for all methods when compared against their standard counterparts. With respect to grid refinement, TKE seems to converge to a level slightly above the W9LM data in Figure 8(b) at late times.

6. Conclusions

This paper has discussed the theoretical framework justifying the use of the Implicit Large Eddy Simulation method for complex turbulent flows. It has first highlighted

the importance of choice of appropriate numerical methods which can both capture shocks, track multiple materials and have minimal dissipation of high wavenumber features in turbulent flows. It has been demonstrated that the ILES methodology can capture canonical flows such as homogeneous decaying turbulence with the appropriate kinetic energy spectrum and kinetic energy decay rates. Simulations of more complex geometries show that the methods can be applied to aeroacoustics problems, swept wing configurations and shock induced turbulent mixing with excellent comparisons to experiment - especially considering the high Reynolds numbers and complex flow physics.

References

Balsara, D.S. & Shu, C.-W. 2000 Monotonicity preserving weighted essentially non-oscillatory schemes with increasingly high order of accuracy. *J. Comput. Phys.* **160**, 405–452, doi: 10.1006/jcph.2000.6443.

Casciola, C.M., Gualtieri, P., Jacob, B. & Piva, R. 2007 The residual anisotropy at small scales in high shear turbulence. *Phys. Fluids* **19**, 101704.

Cohen, R.H., Dannevik, W.P., Dimits, A.M., Eliason, D.E., Mirin, A.A.and Zhou, Y., Porter, D.H. & Woodward, P.R. 2002 Three-dimensional simulation of a Richtmyer-Meshkov instability with a two-scale initial perturbation. *Phys. Fluids* **14** (10), 3692–3709.

Drikakis, D. 2003 Advances in turbulent flow computations using high-resolution methods. *Prog. Aerosp. Sci.* **39**, 405–424, doi:10.1016/S0376-0421(03)00075-7.

Drikakis, D., Fureby, C., Grinstein, F., Hahn, M. & Youngs, D. 2006 MILES of transition to turbulence in the Taylor-Green vortex system. In *ERCOFTAC Workshop on Direct and Large Eddy Simulation-6*, p. 133.

Drikakis, D. & Rider, W. 2004 *High-Resolution Methods for Incompressible and Low-Speed Flows*. Cambridge: Springer Verlag.

Forestier, N., Jacquin, L. & Geffroy, P. 2003 The mixing layer over a deep cavity at high-subsonic speed. *J. Fluid Mech.* **475**, 101–144, doi:10.1017/S0022112002002537.

Fureby, C. & Grinstein, F.F. 2002 Large eddy simulation of high-Reynolds-number free and wall-bounded flows. *J. Comput. Phys.* **181**, 68–97, doi:10.1006/jcph.2002.7119.

Fureby, C., Tabor, F., Weller, H.G. & Gosman, A.D. 1997 A comparative study of subgrid scale models in homogeneous isotropic turbulence. *Phys. Fluids* **9** (5), 1416–1429.

Garnier, E., Mossi, M., Sagaut, P., Comte, P. & Deville, M. 1999 On the use of shock-capturing schemes for large-eddy simulation. *J. Comput. Phys.* **153**, 273–311, doi:10.1006/jcph.1999.6268.

Godunov, S.K. 1959 A finite-difference method for the computation of discontinuous solutions of the equations of fluid dynamics. *Mat. Sb.* **47**, 271–295.

Gordnier, R.E. & Visbal, M.R. 2005 Compact difference scheme applied to simulation of low-sweep delta wing flow. *AIAA J.* **43** (8), 1744–1752.

Grinstein, F.F., Margolin, L.G. & Rider, W.J., ed. 2007 *Implicit Large Eddy Simulation: Computing Turbulent Fluid Dynamics*. Cambridge: Cambridge University Press.

Hahn, M. 2008 Implicit Large-Eddy Simulation of Low-Speed Separated Flows Using High-Resolution Methods. PhD thesis, Cranfield University.

Hahn, M. & Drikakis, D. 2005 Large eddy simulation of compressible turbulence using high-resolution methods. *Int. J. Numer. Meth. Fl.* **49**, 971–977, doi:10.1002/fld.882.

Hickel, S., Adams, N.A. & Domaradzki, J.A. 2006 An adaptive local deconvolution method for implict LES. *J. Comput. Phys.* **213**, 413–436, doi:10.1016/j.jcp.2005.08.017.

Holder, D.A., Smith, A.V., Barton, C.J. & Youngs, D.L. 2003 Shock-tube experiments on Richtmyer-Meshkov instability growth using an enlarged double-bump perturbation. *Laser Particle Beams* **23**, 411–418.

Jameson, A., Schmidt, W. & Turkel, E. 1981 Numerical solutions of the euler equations by finite volume methods using runge-kutta time-stepping schemes. *AIAA 81-1259* .

Jeong, J. & Hussain, F. 1995 On the identification of a vortex. *J. Fluid. Mech.* **285**, 69–94.

Kim, K.H. & Kim, C. 2005 Accurate, efficient and monotonic numerical methods for multi-dimensional compressible flows part II: Multi-dimensional limiting process. *J. Comput. Phys.* **208**, 570–615, doi:10.1016/j.jcp.2005.02.022.

Kolmogorov, A.N. 1941 The local structure of turbulence in an incompressible fluid at very high Reynolds numbers. *Dokl. Akad. Nauk. SSSR* **30**, 299.

Kolmogorov, A.N. 1962 A refinement of previous hypotheses concerning the local structure of turbulence in a viscous incompressible fluid at high Reynolds number. *J. Fluid Mech.* **13**, 82–85.

Larcheveque, L., Sagaut, P., Mary, I. & Labbe, O. 2003 Large-eddy simulation of a compressible flow past a deep cavity. *Phys. Fluids* **15** (1), 193–209, doi:10.1063/1.1522379.

Lesieur, M. & Metais, O. 1996 New trends in large-eddy simulations of turbulence. *Annu. Rev. Fluid Mech.* **28**, 45–82.

Li, N. & Leschziner, M. A. 2007 Large-eddy simulation of separated flow over a swept wing with approximate near-wall modelling. *The Aeronautical Journal* **111** (1125), 689–697.

Margolin, L.G. & Rider, W.J. 2005 The design and construction of implicit LES modes. *Int. J. Numer. Meth. Fl.* **47**, 1173–1179.

Margolin, L.G., Rider, W.J. & Grinstein, F.F. 2006 Modeling turbulent flow with implicit LES. *J. Turbul.* **7** (15), 1–27.

Margolin, L.G., Smolarkiewicz, P.K. & Sorbjan, Z. 1999 Large-eddy simulations of convective boundary layers using nonoscillatory differencing. *Physica D* **133**, 390–397, doi:10.1016/S0167-2789(99)00083-4.

Margolin, L.G., Smolarkiewicz, P.K. & Wyszogrodzki, A.A. 2002 Implicit turbulence modelling for high Reynolds number flows. *J. Fluids Eng.* **124**, 862–867, doi:10.1063/1.1522379.

Meyers, J., Geurts, B.J. & Sagaut, P. 2007 A computational error-assessment of central finite-volume discretizations in large-eddy simulation using a smagorinsky model. *J. Comput. Phys.* **227** (1), 156–173.

Orzag, S.A. & Patterson, G.S. 1972 Numerical simulation of three-dimensional homogeneous isotropic turbulence. *Phys. Rev. Lett.* **28**, 76–79.

Pope, S.B. 2000 *Turbulent Flows*. Cambridge University Press.

Pope, S.B. 2004 Ten questions concerning the large-eddy simulation of turbulent flows. *New Journal of Physics* **6** (35), 1–24.

Porter, D.H., Woodward, P.R. & Pouquet, A. 1998 Inertial range structures in decaying compressible turbulent flows. *Phys. Fluids* **10** (1), 237–245.

Sagaut, P. 2001 *Large Eddy Simulation for Incompressible Flows*. Springer Verlag.

Smolarkiewicz, P.K. & Margolin, L.G. 1998 MPDATA: a finite difference solver for geophysical flows. *J. Comput. Phys.* **140** (2), 459–480, doi:10.1006/jcph.1998.5901.

Spiteri, R.J. & Ruuth, S.J. 2002 A class of optimal high-order strong-stability preserving time discretization methods. *SIAM J. Num. Anal.* **40** (2), 469–491, doi = 10.1137/S0036142901389025.

Thornber, B. & Drikakis, D. 2008 Implicit large eddy simulation of a deep cavity using high resolution methods. *AIAA J.* **46** (10), doi:10.2514/1.36856.

Thornber, B., Drikakis, D., Williams, R. & Youngs, D. 2008*a* On entropy generation and dissipation of kinetic energy in high-resolution shock-capturing schemes. *J. Comput. Phys.* **227**, 4853–4872, doi:10.1016/j.jcp.2008.01.035.

Thornber, B., Mosedale, A. & Drikakis, D. 2007 On the Implicit Large Eddy Simulation of homogeneous decaying turbulence. *J. Comput. Phys.* **226**, 1902–1929, doi:10.1016/j.jcp.2007.06.030.

Thornber, B., Mosedale, A., Drikakis, D., Youngs, D. & Williams, R. 2008*b* An improved reconstruction method for compressible flows with low Mach number features. *J. Comput. Phys.* **227**, 4873–4894, doi:10.1016/j.jcp.2008.01.036.

Toro, E.F. 1997 *Riemann Solvers and Numerical Methods for Fluid Dynamics*. Cambridge: Springer-Verlag.

Zoltak, J. & Drikakis, D. 1998 Hybrid upwind methods for the simulation of unsteady shock-wave diffraction over a cylinder. *Comput. Method. Appl. M.* **162**, 165–185.